Osmotic pressure enables high yield assembly of giant vesicles in solutions of physiological ionic strengths

Alexis Cooper[†], Vaishnavi Girish[§] and Anand Bala Subramaniam[§,*]

† Department of Chemistry and Biochemistry, University of California, Merced, Merced, CA 95343, United States.

§ Department of Bioengineering, University of California, Merced, Merced, CA 95343, United States.

Corresponding Author: asubramaniam@ucmerced.edu

Abstract

Giant unilamellar vesicles (GUVs) are micrometer scale minimal cellular mimics that are useful for synthetic biology and drug delivery. However, their assembly in solutions with ionic concentrations of 100-150 mM Na/KCl (salty solutions) is challenging. Here, we investigate quantitatively the effects of temperature and chemical identity of small molecule compounds and macromolecular polymers on the molar yields of GUVs using high resolution confocal microscopy and large dataset image analysis. The macromolecular polymer low gelling temperature agarose is the singular compound that is effective in producing high yields of GUVs in salty solutions. We propose a free-energy model of budding to explain the effects of polymers in assisting the assembly of GUVs. Experimental data obtained by modulating the ionic strength of the solution support our model's prediction that the osmotic pressure of dissolving polymers results in a net reduction in the free energy for bud formation. The uncovered mechanistic insight provides a quantitative experimental and theoretical framework to guide future studies and shows a facile means for obtaining GUVs in solutions of physiological ionic strengths.

Introduction

Giant unilamellar vesicles, GUVs, vesicles with a single bimolecular wall of phospholipids with diameters ≥ 1 μm, mimic the minimal configuration of biological cells[1,2]. GUVs are useful for bottom-up synthetic biology and biomedical applications[3–12]. Conventionally it has been challenging to obtain GUVs in solutions with ionic concentrations ~100 – 150 mM Na/KCl (salty solutions) using thin-film hydration[1,13,14]. This limitation presents a long standing challenge for the use of GUVs in applications since biomolecules such as proteins, nucleic acids, and polysaccharides require salty solutions to function[15–19].

Several approaches have been proposed to improve the yields of GUVs in salty solutions. Soluble hexoses such as fructose-doped lipids,[20] macromolecular polymeric films composed of ultralow gelling temperature agarose,[21] polyvinyl alcohol (PVA),[22] crosslinked polyacrylamide,[23] and crosslinked dextran(polyethylene glycol)[24] have been used to assist the assembly of GUVs in salty solutions. The relative effectiveness of these various compounds compared to each other and the yields of GUVs that they can produce however is unknown. Importantly, the lack of quantitative data hinders a physicochemical understanding of the mechanism these compounds exert in assisting the assembly of GUVs in salty solutions.

Here, we investigate the molar yields of GUVs in salty solutions as a function of the temperature and chemical identity of the assisting compounds. We performed experiments using the model zwitterionic phospholipid diolyeoyl-*sn*-glycero-3-phosphocholine (DOPC) at two temperatures 22 °C and 37 °C. We evaluated the small molecule fructose, the synthetic macromolecular polymer PVA and four natural macromolecular polysaccharides, agaroses with different degrees of hydroxyethyl substitution. The degree of substitution effects among other properties, the gelling temperature of the agaroses[25,26].

We find that low gelling temperature agarose is the singular compound that produces high yields of GUVs, 17 %, in salty solutions. Although the other polymers were effective in increasing yields in a temperature dependent manner, they only produced moderate to low yields of GUVs, < 10 %. The fructose was ineffective, producing very low yields, < 1 %. This yield was similar to assembly without any assisting compounds. Interestingly, we find via high-resolution single-plane confocal images that surfaces that show circular buds with the largest diameters and highest densities often have the lowest yields of GUVs. Further analysis revealed the presence of polymer-lipid 'pseudobuds' in addition to regular GUV buds. The pseudobuds form due to the dewetting of the polymer films from the surfaces. These pseudobuds morphologically resemble GUV buds but do not produce free-floating giant vesicles.

We develop a free energy model of budding to explain the effects of the macromolecular polymer on the yield of GUVs. High concentration of ions increases the adhesion potential of membranes in lamellar stacks. Our model shows that the gradient in osmotic pressure imposed by the dissolving polymer can balance the increased adhesion potential of the membranes in solutions of high ionic strengths. We test the model by experimentally modulating the adhesion potential using buffers of varying ionic strengths and ion valencies. Our results support the prediction that the osmotic pressure of the dissolving polymer acts to oppose adhesion between membranes. The polymers' contribution to the osmotic pressure results in a net reduction in the free energy for bud formation explaining mechanistically the source of the high yields.

Results and Discussion

Properties of the compounds tested

Figure 1 shows the chemical structure and properties of the compounds that we test. PVA is a water-soluble synthetic polymer composed of vinyl monomer units[27]. The PVA used in this study

has a molecular weight of 146-186 kDa and is 99+% hydrolyzed. Uncrosslinked PVA at 5 wt % or less does not gel and remains a viscous liquid at room temperature[27]. Dehydrated PVA forms a partially soluble swollen polymer film when rehydrated below its glass transition temperature of ~ 85 °C.[27] The solubility of this polymer in water is 6 % at 20 °C and 13 % at 40 °C[27].

Agarose is a naturally derived polysaccharide composed of 1,3-linked β-D-galactopyranose and 1,4-linked 3,6-anhydro-α-L-galactopyranose with an average molecular weight of 120 kDa[28]. Solutions of agarose are conventionally prepared by dissolving 2 wt % or less of agarose powder at elevated temperatures[27]. When the solution is cooled to below the 'gelling' temperature, the agarose polymers transition from random coils into double helices[26]. The double helices hydrogen bond to form a percolated gel network[26]. Heating to above the 'melting' temperature dissolves the gel into a liquid polymeric solution consisting of random agarose coils[29]. Agarose exhibits thermal hysteresis. The melting temperature is significantly higher than the gelling temperature[29]. Synthetic hydroxyethylation can modify the gelling and melting temperature of agarose[25,26]. We refer to the agaroses by the manufacturer's classification as ultralow gelling temperature agarose (ULGT), low gelling temperature agarose (LGT), medium gelling temperature agarose (MGT), and high gelling temperature agarose (HGT). We show the gelling temperatures of the agaroses in Supporting Information Table S1.

Fructose is a highly water soluble small molecule monosaccharide with molecular weight of 180.16 Da[30]. Fructose is thus ~ 600× smaller than PVA and agarose.

Low gelling temperature agarose produces the highest yield of GUVs

We assembled GUVs by hydrating the lipid coated surfaces in a solution of PBS+100 mM sucrose at 22 °C (room temperature) and at 37 °C. The sucrose was necessary to obtain a density gradient for our quantification procedure and is present in all the hydration buffers that we used. After 2

hours of incubation, we harvested the vesicle buds from the surfaces and compare the molar yields of the GUVs. The molar yield measures the moles of lipid in the membranes of the harvested GUVs relative to the moles of lipids deposited on the substrate[31]. The molar yield is an objective measure that allows quantitative comparison of the effects of experimental variables on the yield of GUVs[31]. To isolate the effects of the assisting compounds on assembly in salty solutions, we perform experiments on bare glass surfaces without any assisting compounds in PBS+100 mM sucrose and in a low salt buffer consisting only of 100 mM sucrose.

Figure 2a shows a stacked bar plot of the molar yields obtained at room temperature and Figure 2b shows the molar yields obtained at 37 °C. We divide the yields into small GUVs (diameters d, 1 μm ≤ d < 10 μm), large GUVs (10 μm ≤ d < 50 μm), and very large GUVs (d ≥ 50 μm). The values are a mean of three independent measurements per sample. Error bars are the standard deviation from the mean. We show the full histogram of the distribution of sizes in Supporting Information Figure S1 and S2 and representative images of the harvested vesicles in Supporting Information Figure S3. To assess the statistical significance of the assisting compounds on yields at room temperature, we perform a balanced one-way analysis of variance (ANOVA). The ANOVA showed that at least one of the compounds had a significant effect on the yield of GUVs [$F(7,16) = 230.17$, $p = 7.59\times10^{-15}$]. We performed Tukey's Honestly Significant Difference (HSD) post hoc tests to determine statistical significance between pairs of conditions. A p-value of < 0.05 was considered significant. See Table S2 for the ANOVA table and the results of the Tukey's HSD.

At room temperature, the yields of GUVs from bare glass in a hydrating solution consisting of 100 mM of sucrose is 16.5 ± 0.3%. This result is consistent with previous reports for gentle hydration on glass surfaces[31]. The yield of GUVs that we obtained from the lipids deposited on

bare coverslip surfaces in the buffer containing PBS was ~ 100 times lower, 0.2 ± 0 % ($p = 6.01 \times 10^{-8}$), than the yield in buffer consisting only of sucrose. This result confirms quantitatively that the yield of GUVs is reduced significantly in salty solutions. The fructose-doped lipid and HGT agarose produced a yield of 0.2% and 0.3% which was statistically indistinguishable from bare glass (both $p \geq 0.999$). ULGT agarose, MGT agarose, and PVA produced yields statistically indistinguishable from each other at 2.7 ± 0.2%, 4.8 ± 0.5%, and 5.0 ± 1.0% respectively. These three polymers increase the yield of GUVs modestly compared to assembly on bare glass (all $p < 0.05$). LGT agarose produced the highest yield of GUVs at 17 ± 1%. This yield is more than three times higher than the yield from ULGT agarose, HGT agarose, and PVA. This result is notable since ULGT agarose and PVA, both used extensively in the literature[32–40], produce significantly lower yields of GUVs in PBS compared to LGT agarose. ULGT and LGT agaroses with different catalog numbers showed similar yields to those shown in Figure 2 (Figure S4).

At 37 °C, the ANOVA showed that at least one of the assisting compounds had a significant effect on the yield of GUVs [$F(7,16) = 133.81$, $p = 5.41 \times 10^{-13}$]. See Table S3 for the ANOVA table and the results of the Tukey's HSD, and Table S4 for the Student's t-tests of the effect of temperature. The yield of GUVs on bare glass using the sucrose buffer, 15 ± 1%, was statistically indistinguishable from assembly at room temperature. However, the increased temperature resulted in a statistically significant increase in the yields of GUVs on bare glass in PBS to 1.4 ± 0.4% (p= 0.00480). MGT agarose, PVA, and HGT agarose all showed statistically significant increases in yield compared to assembly at room temperature to 9.0 % ± 0.3% ($p = 0.0224$), 7.6% ± 0.8% ($p = 0.0314$), and 3.8 ± 0.5% ($p = 2.20 \times 10^{-4}$) respectively. The yield of GUVs from PVA and MGT agarose were indistinguishable, and their increased yields compared to HGT agarose was statistically significant. ULGT agarose and the fructose-doped lipid had yields similar to

assembly at room temperature at 3.1 ± 0.1% and 0.2% respectively. Interestingly, the increase in temperature resulted in an almost 9-fold decrease in the yield of GUVs on LGT agarose to 2.0 ± 0.1% ($p = 1.40 \times 10^{-5}$). This dramatic drop in yield for LGT agarose resulted in the yields of GUVs from ULGT agarose, LGT agarose, and the fructose-doped lipid to be statistically indistinguishable from simple gentle hydration in PBS at 37 °C.

To summarize our results, we define semi-quantitative ranges based on the dynamic range of the molar yields. A compound produces a 'high' yield of GUVs if the yields are between 10 – 20%, a 'moderate' yield if the yields are between 5 – 10%, and a 'low' yield if the yields are between 1 – 5%. We consider a compound produces 'very low' yields if the yields are < 1%. Using these metrics, at room temperature and 37 °C, gentle hydration in sucrose produces high yields of GUVs. Gentle hydration in PBS produces very low yields at room temperature and low yields at 37 °C. LGT agarose at room temperature is the *only* polymer that produces a high yield of GUVs in PBS. The other polymers produced moderate to low yields of GUVs even when the temperature was increased to 37 °C. The fructose-doped lipid produced very low yields of GUVs and was ineffective at obtaining a higher yield compared to gentle hydration in PBS.

Characterization of the hydrated lipid films reveals the presence of polymer-lipid pseudobuds

To understand these results, we imaged the lipid-coated surfaces prior to harvesting using high resolution single plane confocal microscopy. We show in Figure 3 the surfaces that have few circular buds. These images are consistent with the very low yields of GUVs that we obtained from these surfaces (Fig. 2). On bare coverslips, we observe flat fluorescent surfaces with stepped differences in intensity and few spherical buds (Fig. 3a). These images are reminiscent of supported lipid bilayers on glass surfaces[41]. We interpret the stepped difference in fluorescence

intensity as overlapping bilayers in a stack. Spherical buds can be seen in typical fields of views on the surfaces incubated at 37 °C compared to surfaces incubated at room temperature (Fig. 3b, white arrow). Images of the fructose-doped lipid did not show any regions that appeared to be lipid bilayers or vesicle buds (Fig. 3c). Instead, the surface was characterized by irregular punctate structures. We interpret these structures as being lipid aggregates. HGT agarose at room temperature showed smooth bilayers on the surface (Fig. 3d).

We find a high density of structures reminiscent of GUV buds on all the other polymer coated surfaces (Fig. 4). Puzzlingly, surfaces that appeared to have a high density of large spherical buds such as PVA and ULGT agarose at room temperature and ULGT, LGT, and MGT agaroses at 37 °C produced relatively low yields of free-floating GUVs. Furthermore, these surfaces often have buds of larger diameters and of higher surface densities compared to the high yielding LGT agarose at room temperature. To understand further why surfaces with high numbers of apparent buds showed low yields of free-floating GUVs, we evaluated the structure of the buds by examining the distribution of fluorescence intensity. GUV buds imaged using confocal microscopy have a uniform fluorescence intensity[31]. Consistent with previous observations, all the buds on surfaces that were incubated in low salt solutions have a uniform distribution of fluorescence intensities (Fig. 5a). On the polymer coated surfaces in PBS, we find two types of structures. Buds with uniform fluorescence intensities reminiscent of GUV buds, (white arrows in Fig. 5b,c) and novel buds with dark regions of low fluorescence intensity (red arrows in Fig. 5b,c). These dark regions had shapes that could be spinodal-like (red arrows Fig. 5b) or circular (red arrows in Fig. 5c). Further, buds that showed these patterns often were larger and had higher membrane fluorescence intensity compared to the buds without dark regions (compare Fig. 5a with Fig. 5d).

Based on these observations, we propose that on polymeric surfaces, two types of buds form. The first are regular GUV buds. The second are hybrid polymer-lipid 'pseudobuds' that nominally resemble GUV buds. We propose that the polymer-lipid pseudobuds arise when the lipid coated polymer film swells and dewets from the surface. This interpretation explains the dark region at the base of the pseudobuds where the polymer has lifted with the lipid. Indeed, the spinodal and circular patterns at the base of the pseudobuds are reminiscent of spinodal and heterogenous nucleation patterns observed for polymer and polysaccharide films that dewet from a supporting substrate[42–45]. Localized dewetting of the polymer film and lifting of the stacks of lipid also explains the high membrane fluorescence intensity of the pseudobuds. The high fluorescence intensity suggests that pseudobuds are composed of multiple lipid bilayers.

We test for the formation of polymer-lipid pseudobuds using the lipid DOPE. DOPE cannot assemble into vesicles because it forms hexagonal phases instead of lamellar phases[46]. We thus expect no GUV buds to form on the surface. We use PVA and ULGT agarose, two surfaces which form a high numbers of pseudobuds. Our images show clear structures resembling pseudobuds, and no structures resembling GUV buds (Figure 6). On harvesting, we obtained no measurable yield of GUVs. We conclude that films of lipids and polymers can form pseudobuds that nominally resemble GUV buds. These pseudobuds are not productive for forming GUVs.

Analysis of our images showed that the number of pseudobuds were lowest for the LGT agarose at room temperature, explaining the high yield of free-floating GUVs from this surface. At 37 °C, the number of pseudobuds on this surface increases at the expense of GUV buds. The increased formation of pseudobuds due to dewetting explains the low yield of free floating GUVs. All the other polymer surfaces have a high number of pseudobuds. Thus, although the surfaces of polymers can appear to be covered with a large number of spherical buds (Figure 4), most of the

buds cannot be harvested to form GUVs. Our discovery of pseudobuds explains previous observations of low yields of free-floating GUVs despite the apparent high number of circular buds on the surfaces[13,22].

Osmotic pressure of dissolving polymers promotes the assembly of GUVs

Currently, there is no consensus on how polymers promote the assembly of GUVs[13,20,22,47]. Upon hydration, lipids assemble into multibilayer stacks that conform to the geometry of the supporting solid substrate[48]. We had previously shown that gentle hydration on surfaces composed of nanoscale cylindrical fibers (nanocellulose paper) resulted in twice the yields of GUVs compared to flat surfaces[31]. We explained this result by showing that the free energy change for the formation of spherical buds from membranes templated on cylindrical fibers was lower than the free energy change from membranes templated on flat surfaces. In conditions where the energy to perform work is fixed, processes with low positive changes in free energies or high negative changes in free energies result in high yields of GUVs[31]. Equation 1 shows the change in free energy for budding on flat surfaces, $\Delta E,$ retaining the pressure-volume term and dropping the edge energy term (See Supporting Information Text for further details).

$$\Delta E = 8\pi\kappa_B - \xi A + \Delta PV \quad (1)$$

In this equation κ_B is the bending rigidity of the membrane, ξ is the adhesion potential between the membranes, A is the area of the bud, ΔP is the difference in osmotic pressure, and V is the volume of the bud. ξ is negative for attractive interactions. Thus, in the absence of an osmotic pressure, that is $\Delta P = 0$, the free energy change for the formation of buds is always positive[31]. External energy due to hydrodynamic flows or temperature gradients[49] provide work to form GUV buds.

Our data shows that in PBS, the yields of GUVs on flat surfaces is very low (Fig. 2a). This result suggests that the external energy due to flows and temperature gradients, which was sufficient to produce high yields of GUVs in low salt solutions, is insufficient to form GUVs in PBS. Dissolved ions increase adhesion between surfaces in aqueous solutions by screening electrostatic charges[46,50]. Examination of Equation 1 shows that an increase in the magnitude of the adhesion potential, ξ, increases the energy required to form a bud. This increase in the magnitude of required energy to form buds due to electrostatic screening is expected to decrease the number of buds formed. This result is consistent with our observed dramatic decrease in the yield of GUVs obtained through gentle hydration in PBS compared to low salt solutions (the leftmost bars in Fig. 2a).

For polymer coated surfaces, dissolution of the polymer can create a difference in osmotic pressure in the interlamellar space of the bilayer stacks. The osmotic pressure acts in the opposite direction to the adhesion potential since there is a high concentration of polymers on the surface and no polymers in the bulk solution. Thus ΔP is non-zero and negative. The negative third term in the right-hand side of Equation 1 allows the possibility for no change or even a net decrease in free energy that can balance an increase in the magnitude of the adhesion energy due to an increase in the ionic concentrations.

Since it is challenging to measure the dissolution of small amounts of polymer, we devise experiments to probe for the effects of osmotic pressure by modulating the magnitude of the adhesion potential of the membranes relative to PBS. Equation 1 shows that for a fixed non-zero and negative osmotic pressure and constant bud volume, the magnitude and sign of ΔE depends only on the magnitude of the adhesion potential. The adhesion potential between membranes is lowest in solutions of low ionic strength. High concentrations of monovalent ions reduce the

double layer screening length[46,50], while mM concentrations of divalent cations can neutralize surface charges or function as ionic bridges[51,52]. These conditions promote adhesion between membranes[50,53,54] (See Supporting Information Text, Table S5, Table S6 for further discussion and calculations of the double layer screening length). We reduced the adhesion potential relative to PBS by using 100 mM sucrose with no added salts and increased the adhesion potential by using 600 mM NaCl, a solution with a monovalent salt concentration that is more than four times that of PBS. We also used buffers with mM amounts of the divalent cations Mg^{2+} and Ca^{2+}, PBS + 5 mM $MgCl_2$ and 150 mM KCl + 5 mM $CaCl_2$. The combinations of salts served to test for generality.

Figure 7 shows the molar yields obtained from LGT agarose in the solutions. The yield of GUVs was affected significantly by the composition of the hydrating buffer [$F(4,10) = 196.32$, $p = 1.87 \times 10^{-9}$]. See Table S7 for the ANOVA table and the results of the Tukey's HSD. In solutions devoid of salt, the yield of GUVs from LGT doubled to 40 ± 3% compared to assembly in PBS ($p = 1.43 \times 10^{-7}$). In 600 mM NaCl, PBS + 5 mM $MgCl_2$, and 150 mM KCl + 5 mM $CaCl_2$, the yield was approximately halved to 6.0 ± 1.0 % ($p = 8.14 \times 10^{-5}$), 9.0 ± 1.0 % ($p = 0.00124$), and 9.0 ± 1.0% ($p = 0.00137$) respectively. Clearly, buffers that decrease the adhesion potential result in an increase in the yield while buffers that increase the adhesion potential result in a decrease in the yield. These results are consistent with the osmotic pressure of dissolving polymers as the mechanism behind the formation of GUVs on polymer-coated surfaces.

Insights into obtaining high yields of GUVs in solutions of physiological ionic strengths Our results show that small molecule sugars are ineffective at increasing yields. Note that the very low yields that we find here are consistent with data from previous reports[21] (Supporting Information Text). We propose that the high solubility of sugars and their small size allows them to escape

through defects in the bilayer, making sugars unable to exert an osmotic pressure against the membrane.

For PVA, MGT, and HGT agaroses, the low solubility of the polymer at room temperature is consistent with the low to very low yields of free-floating GUVs. Increasing the temperature increases the solubility of the polymer resulting in an increase in the yield of GUVs. LGT agarose at 22 °C appears to be unique. It is the only polymer that can produce high yields of GUVs in salty solutions.

LGT and ULGT agaroses have synthetic hydroxyethyl groups[25,26]. These hydrophobic groups lower the gelling and melting temperatures by decreasing the number of intrastrand hydrogen bonds that can form between the polymer chains[25,26]. We propose that the degree of hydrophobic modification of the LGT agarose polymer chain is ideal for interacting with the lipid during the preparation of the lipid films. This ideal interaction results in effective dissolution of the polymer between the interlamellar space of the bilayer stacks upon hydration. At 37 °C, which is above the gelling temperature of LGT agarose, dewetting from the substrate to form large numbers of pseudobuds significantly decreases yields. The low yields of ULGT agarose and the large numbers of pseudobuds on the surface is consistent with dewetting. We conclude that an optimal polymer chemistry, and selection of temperatures that allows dissolution while minimizing dewetting, is necessary to obtain high yields of GUVs.

Since dissolution of the polymer appears to be key for the formation of GUVs in salty solutions, extrapolating from our results of PVA, cross-linking polymers to minimize dissolution will likely result in moderate to low yields of GUVs in buffers of physiological ionic strengths.

Conclusion

Quantitative experiments revealed that the formation of GUVs from films of DOPC in PBS depends significantly on the chemistry of the polymers and the assembly temperature. LGT agarose at room temperature produced the highest yield of free floating GUVs in salty solutions. All other polymers produced moderate to low yields of GUVs. Experiments with solutions of varying ionic strengths shows that the difference in osmotic pressure due to dissolving polymers promotes the formation of GUVs. Hydrophobic interactions between LGT agarose and the lipid, in addition to assembly at temperatures that minimize polymer dewetting, significantly increases the yield of GUVs, and is required for high yields. Looking forward, we propose that our free energy model provides a mechanistic guide for future rational studies for discovering polymers that can further improve yields, for example of GUVs that are composed of amphiphilic block copolymers[55,56] or lipids with charged head groups[57].

Methods

Materials

We purchased glass coverslips (Corning, 22 mm × 22 mm) and premium plain glass microscope slides (75 mm × 25 mm) from Thermo Fisher Scientific (Waltham, MA).

Chemicals

We purchased sucrose (BioXtra grade, purity ≥ 99.5%), glucose (BioXtra grade, purity ≥ 99.5%), potassium chloride (molecular biology grade, ≥ 99.0%), magnesium chloride (purity ≥ 98%), casein from bovine milk (BioReagent grade), agarose type IX-A: ultra-low gelling temperature (Catalog number: A2576, molecular biology grade), agarose: low gelling point (Catalog number: A9414, molecular biology grade), agarose type II-A medium EEO (Catalog number: A9918), agarose type VI-A: high gelling temperature (Catalog number: A7174), ultra-low gelling

temperature agarose (Catalog number: A5030), low gelling temperature agarose (Catalog number: A0701) and poly(vinyl alcohol) (M_W 146,000 – 186,000 99+% hydrolyzed) (PVA) from Sigma-Aldrich (St. Louis, MO). We purchased chloroform (ACS grade, purity ≥ 99.8%, with 0.75% ethanol as preservative), Invitrogen 10× PBS Buffer (pH 7.4, 0.2 μm filtered, 1.37 M sodium chloride, 0.027 M potassium chloride, 0.080 sodium phosphate dibasic, 0.020 M potassium phosphate monobasic), sodium chloride (BioXtra grade, purity ≥99.5%) and D-(-)-Fructose (HPLC grade, purity ≥99%) from Thermo Fisher Scientific (Waltham, MA). We obtained 18.2 MΩ ultrapure water from an ELGA Pure-lab Ultra water purification system (Woodridge, IL). We purchased 1,2- dioleoyl-*sn*-glycero-3-phosphocholine (18:1 (Δ9-cis) PC (DOPC)), 23-(dipyrrometheneboron difluoride)-24-norcholesterol (TopFluor-Chol), 1,2-dioleoyl-*sn*-glycero-3-phosphoethanolamine (DOPE) and 1,2-distearoyl-*sn*-glycero-3-phosphoethanolamine-N-[methoxy(polyethylene glycol)-2000](ammonium salt) (18:0 PEG2000-PE) from Avanti Polar Lipids, Inc. (Alabaster, AL).

Lipid mixtures

Lipid mixtures were prepared as previously described with minor adaptations[31]. Briefly, we prepared working solutions of 96.5:3:0.5 mol% DOPC:PEG2000-PE:TopFluor-Chol and 96.5:3:0.5 DOPE:PEG2000PE:TopFluor-Chol at a concentration of 1 mg/mL. All lipid solutions were stored in Teflon-capped glass vials, purged with argon, and stored in a -20°C freezer. Lipid solutions were remade weekly.

Formation of polymer films on glass. Films of polymer on glass coverslips (Corning, 22 mm x 22 mm) were prepared by applying 300 μL of 1 wt % (w/w) polymer on a coverslip and evenly spreading the solution with the side of a pipette tip[56]. The coated glass coverslips were allowed to

dehydrate on a hotplate for a minimum of 2 hours set at a temperature of 40 °C. At the end of the process the coverslip appeared flat and clear.

Deposition of lipids

To ensure standardized conditions that allows comparison between samples, we deposit lipid solutions as described previously[31]. Briefly, circular disks with a diameter of 9.5 mm were traced on the underside of the polymer-coated coverslip, or bare coverslips using a template made from a circle hole punch (EK Tools Circle Punch, 3/8 in.). We evenly deposited 10 μL of the lipid working solution onto the polymer-coated or bare side of the glass within the traced area using a glass syringe (Hamilton). All lipid coated substrates were placed into a laboratory vacuum desiccator for 1 hour to remove any traces of organic solvent before hydration.

Procedure for assembly

Circular poly(dimethyl)siloxane (PDMS) gaskets (inner diameter × height = 12 × 1 mm) were affixed to bare coverslips or polymer coated coverslips to construct a barrier around the dry solvent-free lipid films. We added 150 μL of PBS doped with 100 mM sucrose into the gaskets. To minimize evaporation, we place the gaskets and a water saturated Kimwipe in a sealed 150 mm diameter Petri dish. The films were allowed to hydrate for 2 hours on a laboratory bench at room temperature. For assembly at 37 °C, we preheated the buffers to 37 °C in a water bath. The films were allowed to hydrate for 2 hours on a hotplate set to 37°C. To prevent evaporation, we covered the gaskets with cover slips, and placed the gaskets and a water saturated Kimwipe in a sealed 150 mm diameter Petri dish.

Fructose-doped lipid method

Following a previously published protocol[20], we prepared 1 mM (0.785 mg/mL) DOPC:TopFluor-Chol at 99.5:0.5 mol % in chloroform and 20 mM fructose dissolved in neat methanol. We mixed

50 μL of 1 mM 99.5:0.5 mol % DOPC:TopFluor-Chol in chloroform with 25 μL of 20 mM fructose in methanol to create a 2:1 chloroform:methanol working solution. We applied 15 μL of the solution onto the coverslip and place the coverslip in a vacuum chamber for 1 hour. The dried lipid film was then hydrated in PBS doped with 100 mM sucrose.

Procedure for harvesting the GUVs

Harvesting GUVs from the substrated was conducted as previously described [31]. Briefly, the GUVs were harvested by pipetting 100 μL of the hydrating solution with a cut 1000 μL pipet tip on 6 different regions of the lipid-coated surface to cover the whole area. We aspirated all the GUV containing liquid on the seventh time and transferred the liquid into a 0.5 mL Eppendorf tube. The final sample volume was ~150 μL. Aliquots were taken immediately for imaging.

Confocal microscopy of harvested vesicles

Imaging of harvested vesicles was conducted as previously described[31]. Briefly, we constructed imaging chambers by placing PDMS gaskets with a square opening (width × length × height = 6 × 6 × 1 mm) on glass microscope slides. Before use, we passivated the chamber with a solution of 1 mg/mL casein in PBS to prevent the rupture of GUVs on the surface of bare glass. Chambers were thoroughly rinsed with ultrapure water after passivation. We filled the passivated chamber with 58 μL of a 100 mM solution of glucose in PBS and evenly distributed a 2 μL aliquot of harvested GUV suspension into the 100 mM glucose in PBS solution by repeatedly pipetting 2 μL of the mixed suspension in glucose. We allowed the GUVs to sediment for 3 hours in a sealed 150 mm Petri dish with a water saturated Kimwipe to prevent evaporation before imaging. We captured images using an upright confocal laser-scanning microscope (LSM 880, Axio Imager.Z2m, Zeiss, Germany), using a 488 nm argon laser and a 10× Plan-Apochromat objective with a numerical aperture of 0.45. We imaged using an automated tile scan routine (64 images [850.19 μm × 850.19

μm (3212 pixels × 3212 pixels)]) to capture the entire area of the chamber. The routine used an autofocus feature at each tile location. Out of focus tiles were imaged manually. The pinhole was set at 15.16 Airy units which gave a confocal slice thickness of 79.3 μm.

Imaging the surface of hydrated lipid films

We captured images of the surfaces using an upright confocal laser-scanning microscope (LSM 700, Axio Imager.Z2m, Zeiss, Germany), a diode-488 nm laser and a 10× Plan-Apochromat objective with a numerical aperture of 0.45. The frame size was 2048 pixels × 2048 pixels. The pinhole was set to 1 Airy Unit which gave a confocal slice thickness of 5.9 μm. Images were selected to be representative of the whole surface.

Image processing and analysis

We conducted image processing and analysis as previously described[31]. Briefly, we used a custom MATLAB (Mathworks Inc., Natick, MA) routine to analyze the confocal tile scan images. The routine segmented fluorescent objects from the background. To obtain the diameters and mean intensities of the objects, we used the native *regionprops* function. We used the coefficient of variance of the intensities to select GUVs from the detected fluorescent objects All images were inspected after automated segmentation and erroneously segmented objects were manually corrected.

Statistical analysis

All statistical analysis was performed using MATLAB. We conducted 1-way balanced analysis of variance (ANOVA) in MATLAB to determine the statistical significance of the mean yields obtained for the different compounds at a given temperature. We conduct a posthoc Tukey's Honestly Significant Difference (HSD) to determine statistical significance of the differences in

the mean between pairs of surfaces. To compare statistical significance of the difference of temperature on the yields we conduct Student's t-tests.

ASSOCIATED CONTENT

Supporting Information.

The Supporting Information is available free of charge on the ACS Publications website at DOI:

Supporting text describing mathematical details of the molar yield calculations and free-energy model. Figures showing: Histograms of GUV diameters from different substrates. Confocal images of harvested, free-floating GUVs. Tables showing: Compounds tested, p-values for statistical tests, concentrations of salts in buffers, and calculated Debye screening lengths. Figure S1-S6, Table S1-S7, Equation S1-S4. (PDF).

AUTHOR INFORMATION

Corresponding Author

*E-mail: asubramaniam@ucmerced.edu

Author contributions

A.B.S conceived and directed the study. A.C. performed most of the experiments. V.G. performed experiments in Fig. 7. A.C analyzed the data. A.B.S. and A.C. interpreted the data. A.C. prepared the figures and wrote the first draft of the manuscript. A.B.S wrote the final draft. All authors have given approval to the final version of the manuscript.

Acknowledgements

This work was funded by the National Science Foundation through NSF CAREER DMR-1848573, The data in this work was collected, in part, with a confocal microscope acquired through the National Science Foundation MRI Award Number DMR-1625733.

Conflict of Interest

The authors declare no conflict of interest.

References

1. Walde, P., Cosentino, K., Engel, H. & Stano, P. Giant Vesicles: Preparations and Applications. *ChemBioChem* **11**, 848–865 (2010).
2. Gözen, I. *et al.* Protocells: Milestones and Recent Advances. *Small* **18**, (2022).
3. Perrier, D. L., Rems, L. & Boukany, P. E. Lipid vesicles in pulsed electric fields: Fundamental principles of the membrane response and its biomedical applications. *Adv. Colloid Interface Sci.* **249**, 248–271 (2017).
4. Krinsky, N. *et al.* Synthetic Cells Synthesize Therapeutic Proteins inside Tumors. *Adv. Healthc. Mater.* **7**, 1–10 (2018).
5. Li, Q., Li, S., Zhang, X., Xu, W. & Han, X. Programmed magnetic manipulation of vesicles into spatially coded prototissue architectures arrays. *Nat. Commun.* **11**, 1–9 (2020).
6. Staufer, O., Schroter, M., Platzman, I. & Spatz, J. P. Bottom-Up Assembly of Functional Intracellular Synthetic Organelles by Droplet-Based Microfluidics.pdf. *Small* **16**, 190624 (2020).
7. Wang, X., Du, H., Wang, Z., Mu, W. & Han, X. Versatile Phospholipid Assemblies for Functional Synthetic Cells and Artificial Tissues. *Adv. Mater.* **33**, 1–23 (2021).
8. Lussier, F., Staufer, O., Platzman, I. & Spatz, J. P. Can Bottom-Up Synthetic Biology Generate Advanced Drug-Delivery Systems? *Trends Biotechnol.* **39**, 445–459 (2021).
9. Staufer, O. *et al.* Microfluidic production and characterization of biofunctionalized giant unilamellar vesicles for targeted intracellular cargo delivery. *Biomaterials* **264**, 120203 (2021).
10. Pick, H., Alves, A. C. & Vogel, H. Single-Vesicle Assays Using Liposomes and Cell-Derived Vesicles: From Modeling Complex Membrane Processes to Synthetic Biology and Biomedical Applications. *Chem. Rev.* **118**, 8598–8654 (2018).
11. Teixeira, L. *et al.* Use of giant unilamellar lipid vesicles as antioxidant carriers in in vitro culture medium of bovine embryos. *Sci. Rep.* 1–12 (2022).
12. Bansal, S. *et al.* Discovery and Characterization of a Potent Antifungal Peptide through One-Bead, One-Compound Combinatorial Library Screening. *ACS Infect. Dis.* (2022).
13. Stein, H., Spindler, S., Bonakdar, N., Wang, C. & Sandoghdar, V. Production of isolated

giant unilamellar vesicles under high salt concentrations. *Front. Physiol.* **8**, 1–16 (2017).

14. Has, C. & Sunthar, P. A comprehensive review on recent preparation techniques of liposomes A comprehensive review on recent preparation techniques of liposomes. *J. Liposome Res.* **30**, 336–365 (2020).
15. Jørgensen, I. L., Kemmer, G. C. & Pomorski, T. G. Membrane protein reconstitution into giant unilamellar vesicles: a review on current techniques. *Eur. Biophys. J.* **46**, 103–119 (2017).
16. Shaklee, P. M. *et al.* Protein incorporation in giant lipid vesicles under physiological conditions. *ChemBioChem* **11**, 175–179 (2010).
17. Tan, Z. J. & Chen, S. J. Nucleic acid helix stability: Effects of salt concentration, cation valence and size, and chain length. *Biophys. J.* **90**, 1175–1190 (2006).
18. Fischer, A., Franco, A. & Oberholzer, T. Giant Vesicles as Microreactors for Enzymatic mRNA Synthesis. *ChemBioChem* **3**, 409–417 (2002).
19. Girod, S., Cara, L., Maillols, H., Salles, J. P. & Devoisselle, J. M. Relationship between conformation of polysaccharides in the dilute regime and their interaction with a phospholipid bilayer. *Luminescence* **16**, 109–116 (2001).
20. Tsumoto, K., Matsuo, H., Tomita, M. & Yoshimura, T. Efficient formation of giant liposomes through the gentle hydration of phosphatidylcholine films doped with sugar. *Colloids Surfaces B Biointerfaces* **68**, 98–105 (2009).
21. Horger, K. S., Estes, D. J., Capone, R. & Mayer, M. Films of agarose enable rapid formation of giant liposomes in solutions of physiologic ionic strength. *J. Am. Chem. Soc.* **131**, 1810–1819 (2009).
22. Weinberger, A. *et al.* Gel-assisted formation of giant unilamellar vesicles. *Biophys. J.* **105**, 154–164 (2013).
23. Parigoris, E. *et al.* Facile generation of giant unilamellar vesicles using polyacrylamide gels. *Sci. Rep.* **10**, 1–10 (2020).
24. Mora, N. L. *et al.* Evaluation of dextran(ethylene glycol) hydrogel films for giant unilamellar lipid vesicle production and their application for the encapsulation of polymersomes. *Soft Matter* **13**, 5580–5588 (2017).
25. B. Guiseley, K. The relationship between methoxyl content and gelling temperature of agarose. *Carbohydr. Res.* **13**, 247–256 (1970).

26. Lonza Group. Agarose Physical Chemistry. *Agarose Phys. Chem.* 207–209 (2010).
27. Hassan, C. M. & Peppas, N. A. Structure and applications of poly(vinyl alcohol) hydrogels produced by conventional crosslinking or by freezing/thawing methods. *Adv. Polym. Sci.* **153**, 37–65 (2000).
28. Rochas, C. & Lahaye, M. Average molecular weight and molecular weight distribution of agarose and agarose-type polysaccharides. *Carbohydr. Polym.* **10**, 289–298 (1989).
29. Sigma Aldrich. Agarose Product Information.
30. Mark, L. & White, S. Manufacturing, composition and applications of fructose. *Am. J. Clin. Nutr.* **58**, 724S-732S (1993).
31. Pazzi, J. & Subramaniam, A. B. Nanoscale Curvature Promotes High Yield Spontaneous Formation of Cell-Mimetic Giant Vesicles on Nanocellulose Paper. *ACS Appl. Mater. Interfaces* **12**, 56549–56561 (2020).
32. Walpole, G. F. W. *et al.* Kinase-independent synthesis of 3-phosphorylated phosphoinositides by a phosphotransferase. *Nat. Cell Biol.* **24**, 708–722 (2022).
33. Matos, A. L. L. *et al.* CHIMs are versatile cholesterol analogs mimicking and visualizing cholesterol behavior in lipid bilayers and cells. *Commun. Biol.* **4**, (2021).
34. Michels, L. *et al.* Molecular sensors reveal the mechano-chemical response of Phytophthora infestans walls and membranes to mechanical and chemical stress. *Cell Surf.* **8**, 100071 (2022).
35. Eisenberg, S. *et al.* Mapping the electrostatic profiles of cellular membranes. *Mol. Biol. Cell* **32**, 301–310 (2021).
36. Liu, Z., Cui, J. & Zhan, W. Rapid Access to Giant Unilamellar Liposomes with Upper Size Control: Membrane-Gated, Gel-Assisted Lipid Hydration. *Langmuir* **36**, 13193–13200 (2020).
37. Wójcik, A. *et al.* Interactions of polycyclic aromatic hydrocarbons and their nitro derivatives with bilayer and monolayer models of fungal membranes. **360**, (2022).
38. Abdul, S. *et al.* Structural insights into the interaction of antifungal peptides and ergosterol containing fungal membrane. *BBA - Biomembr.* **1864**, 183996 (2022).
39. Gutierrez, M. G. & Malmstadt, N. Human serotonin receptor 5-HT1A preferentially segregates to the liquid disordered phase in synthetic lipid bilayers. *J. Am. Chem. Soc.* **136**, 13530–13533 (2014).

40. Hawkins, W. D. *et al.* Dimerization-dependent membrane tethering by Atg23 is essential for yeast autophagy. *Cell Rep.* **39**, 110702 (2022).
41. Faysal, K. M. R., Park, J. S., Nguyen, J., Garcia, L. & Subramaniam, A. B. Lipid bilayers are long-lived on solvent cleaned plasma-oxidized poly(dimethyl) siloxane (ox-PDMS). *PLoS One* **12**, (2017).
42. Higgins A. M. & Jones R. A. L. Anisotropic spinodal dewettingas a route to self-assembly of patterned surfaces. *Nature* **404**, 476–478 (2000).
43. Xie, R., Karim, A., Douglas, J. F., Han, C. C. & Weiss, R. A. Spinodal dewetting of thin polymer films. *Phys. Rev. Lett.* **81**, 1251–1254 (1998).
44. Xue, L. & Han, Y. Pattern formation by dewetting of polymer thin film. *Prog. Polym. Sci.* **36**, 269–293 (2011).
45. Subramaniam, A. B., Guidotti, G., Manoharan, V. N. & Stone, H. A. Glycans pattern the phase behaviour of lipid membranes. *Nat. Mater.* **12**, 128–33 (2013).
46. Israelachvili, J. N. *Intermolecular and Surface Forces*. *Intermolecular and Surface Forces: Third Edition* (Academic Press, 2011).
47. Yamada, N. L., Hishida, M., Seto, H., Tsumoto, K. & Yoshimura, T. Unbinding of lipid bilayers induced by osmotic pressure in relation to unilamellar vesicle formation. *EPL* **80**, (2007).
48. Tayebi, L. *et al.* Long-range interlayer alignment of intralayer domains in stacked lipid bilayers. *Nat. Mater.* **11**, 1074–1080 (2012).
49. Lasic, D. D. The spontaneous formation of unilamellar vesiscles. *J. Colloid Interface Sci.* **124**, 428–435 (1988).
50. Marra, J. & Israelachvili, J. Direct Measurements of Forces between Phosphatidylcholine and Phosphatidylethanolamine Bilayers in Aqueous Electrolyte Solutions. *Biochemistry* **24**, 4608–4618 (1985).
51. Kucerka, N. *et al.* Cation-zwitterionic lipid interactions are affected by the lateral area per lipid. *Langmuir* (2021). doi:10.1021/acs.langmuir.0c02876
52. Kurakin, S. A., Ermakova, E. V., Ivankov, A. I., Smerdova, S. G. & Kučerka, N. The Effect of Divalent Ions on the Structure of Bilayers in the Dimyristoylphosphatidylcholine Vesicles. *J. Surf. Investig.* **15**, 211–220 (2021).
53. Sun, Y., Lee, C. & Huang, H. W. Adhesion and Merging of Lipid Bilayers : A Method for

Measuring the Free Energy of Adhesion and Hemifusion. *Biophysj* **100**, 987–995 (2011).

54. Leckband, D. E., Helm, C. A. & Israelachvili, J. Role of Calcium in the Adhesion and Fusion of Bilayers. *Biochemistry* **32**, 1127–1140 (1993).
55. Li, A., Pazzi, J., Xu, M. & Subramaniam, A. B. Cellulose Abetted Assembly and Temporally Decoupled Loading of Cargo into Vesicles Synthesized from Functionally Diverse Lamellar Phase Forming Amphiphiles. *Biomacromolecules* **19**, 849–859 (2018).
56. Greene, A. C. *et al.* The Role of Membrane Fluidization in the Gel-Assisted Formation of Giant Polymersomes. *PLoS One* **11**, e0158729 (2016).
57. Peruzzi, J., Gutierrez, M. G., Mansfield, K. & Malmstadt, N. Dynamics of Hydrogel-Assisted Giant Unilamellar Vesicle Formation from Unsaturated Lipid Systems. *Langmuir* **32**, 12702–12709 (2016).
58. Gu, Y., Cheong, K. L. & Du, H. Modification and comparison of three Gracilaria spp. agarose with methylation for promotion of its gelling properties. *Chem. Cent. J.* **11**, 1–10 (2017).
59. Guiseley, K. Modified Agarose and Agar and Method of Making Same. U.S. Patent 3956273. (1976).

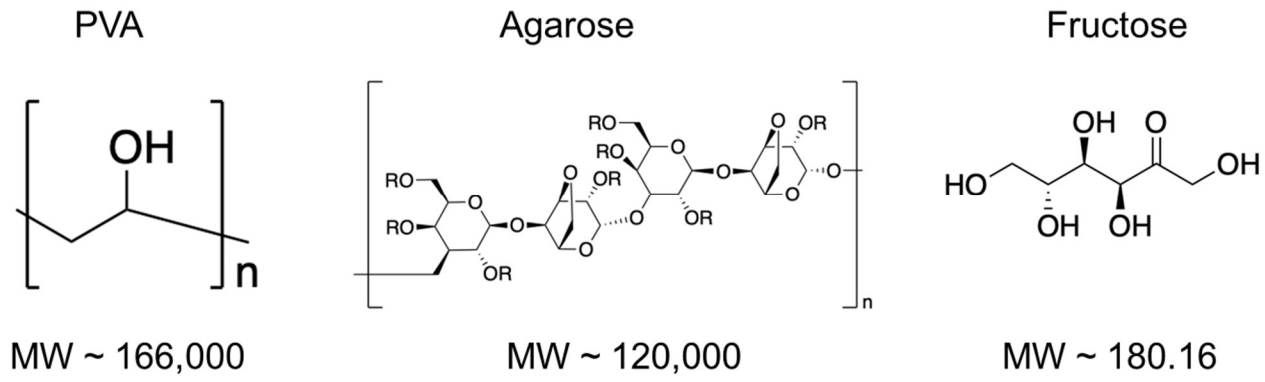

Figure 1. Structural formulas and molecular weight of the compounds. Structural formula of agarose[58,59] R = H, CH_3 or CH_2CH_2OH [26].

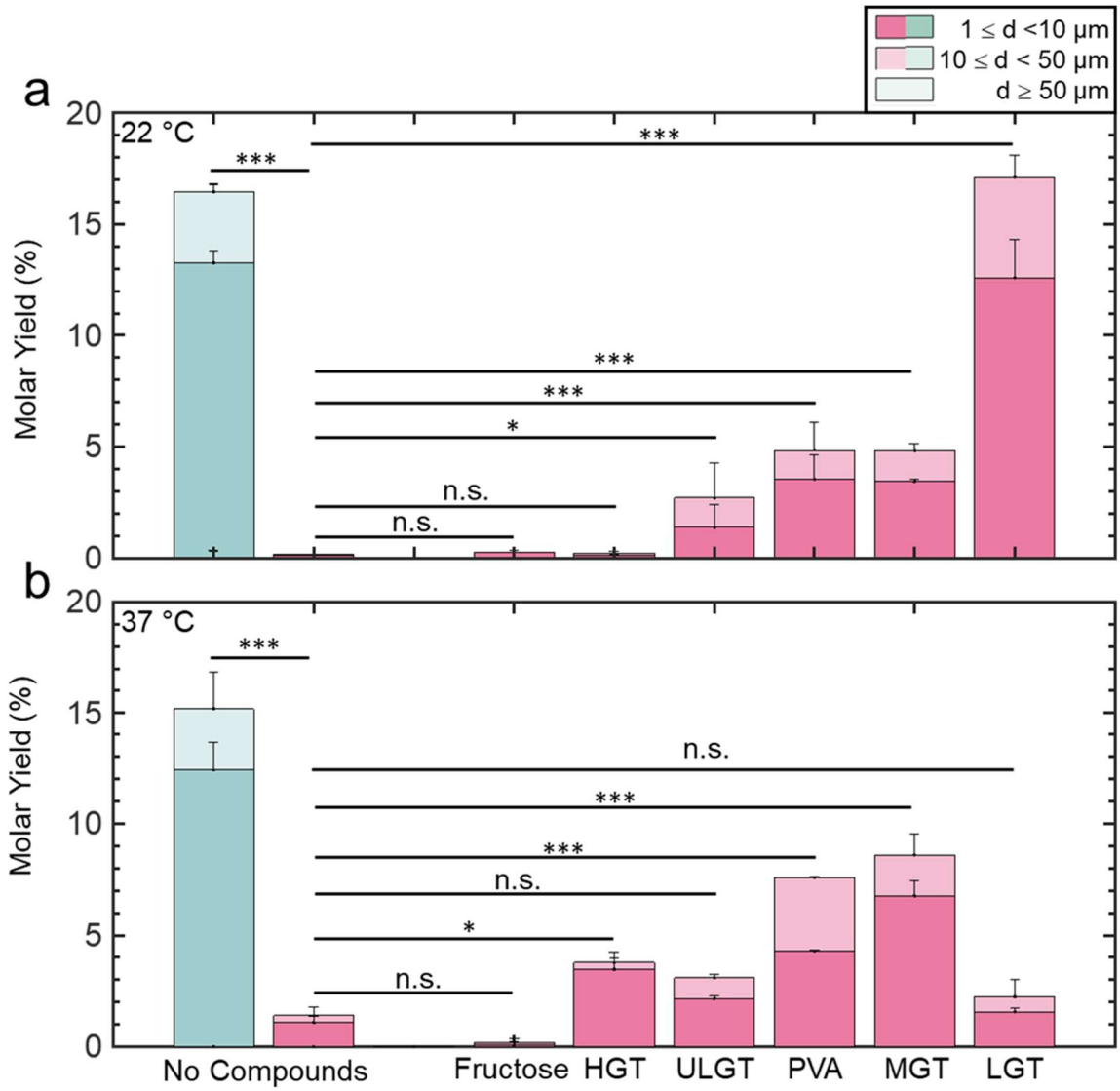

Figure 2. Stacked bar plots of the molar yields of GUVs in salty solutions. The blue bar is for samples hydrated in a low salt solution consisting of 100 mM of sucrose. The red bars are molar yields for samples hydrated in PBS doped with 100 mM sucrose. The two leftmost bars show the molar yield without any assisting compounds. a) Assembly at 22 °C. b) Assembly at 37 °C. Each bar is split into 3 regions corresponding to the diameter ranges specified in the legend. Statistical significance was determined using a balanced one-way ANOVA and Tukey's HSD post hoc tests. * = $p < 0.05$, ** = $p < 0.01$, *** = $p < 0.001$, ns = not significant. LGT agarose is the singular compound that produced high yields of GUVs in salty solutions.

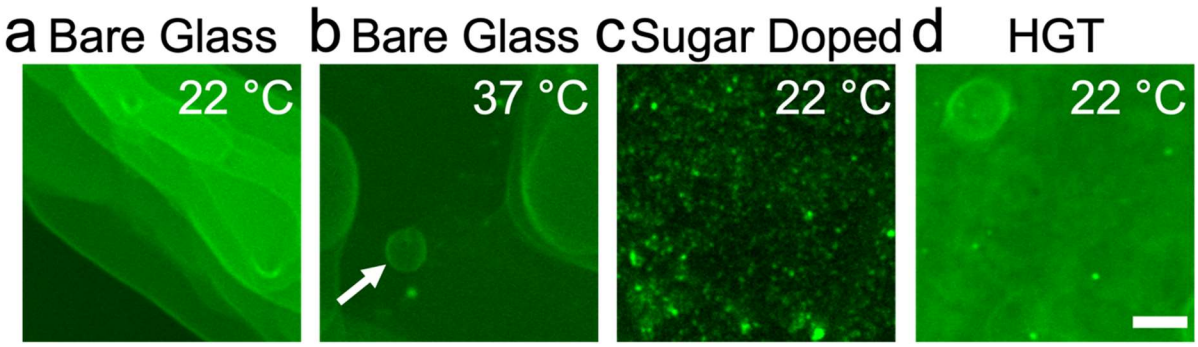

Figure 3. Surfaces that show little to no spherical buds. All samples hydrated in PBS doped with 100 mM sucrose. a) Bare glass, 22 °C, b) bare glass, 37 °C. White arrow points to a spherical bud. c) Sugar-Doped, 22 °C, d) HGT agarose, 22 °C. The scale bar is 15 µm.

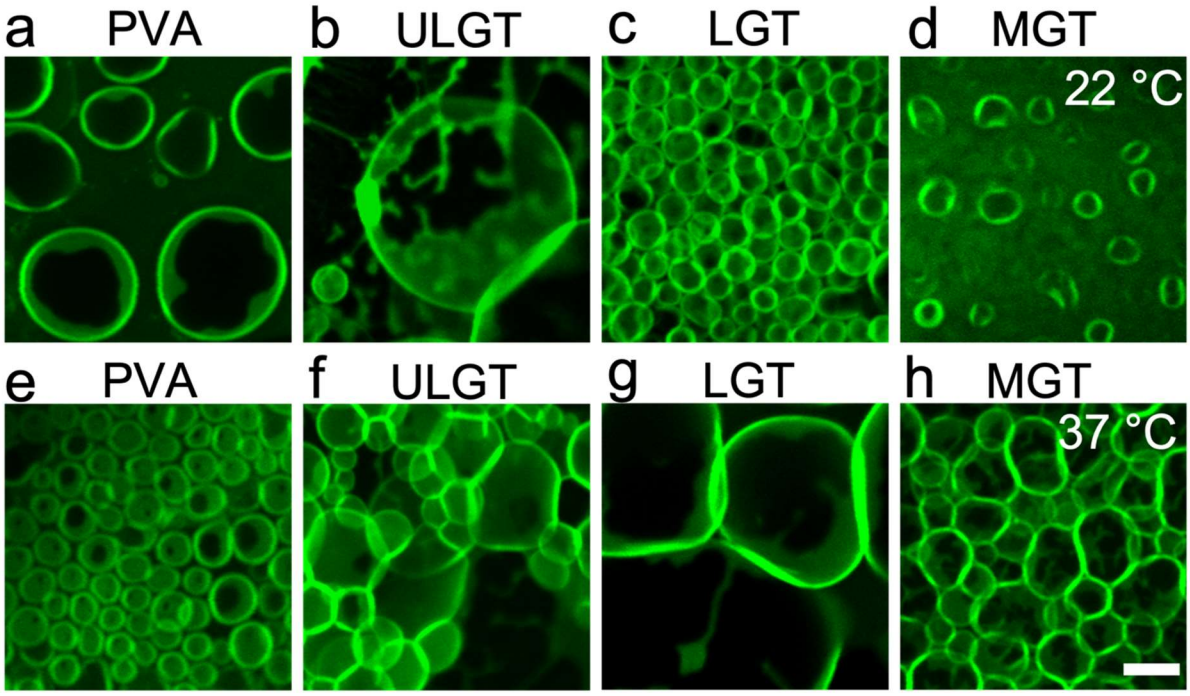

Figure 4. Surfaces that show circular buds. The top row shows images from samples hydrated at 22 °C. The bottom row shows images from samples hydrated at 37 °C. All samples hydrated in PBS doped with 100 mM of sucrose. The scale bar is 15 µm.

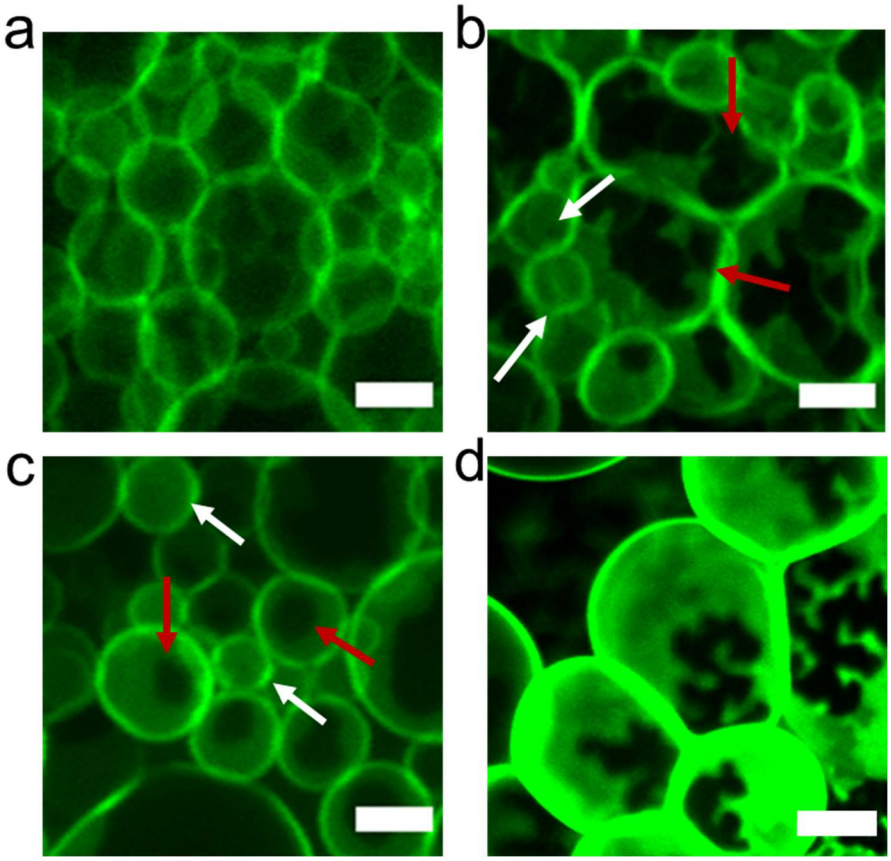

Figure 5. Polymer surfaces form pseudobuds as well as GUV buds. a) Spherical GUV buds with uniform fluorescence intensity as seen in on LGT agarose hydrated in 100 mM sucrose. b) Pseudobuds with spinodal dewetting pattern on LGT agarose (red arrows). GUV buds are highlighted by the white arrows. c) Pseudobuds with circular dewetting pattern on PVA (red arrows). White arrows point to regular GUV buds. d) Large pseudobuds with high fluorescence intensity on ULGT agarose. b-d hydrated in PBS doped with 100 mM sucrose. The scale bars for a-c are 10 µm. The scale bar for d is 20 µm.

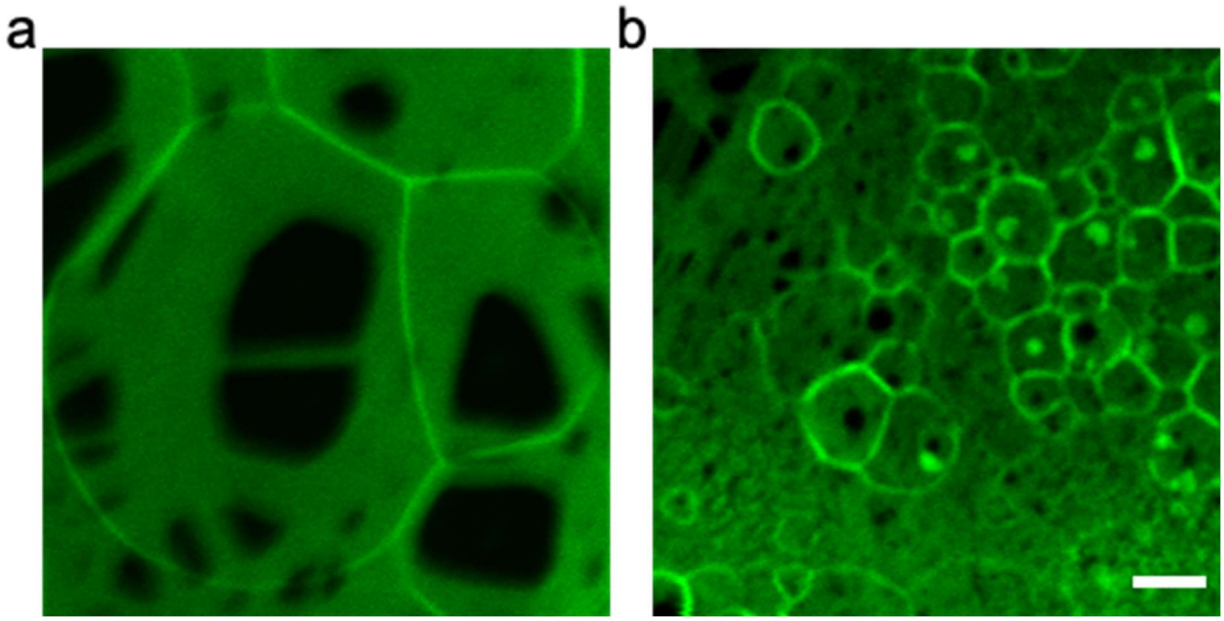

Figure 6. DOPE forms pseudobuds on ULGT agarose and PVA. a) Pseudobuds formed from DOPE on ULGT agarose showing regions of dewetting with low fluorescence intensity. b) Pseudobuds formed from DOPE on PVA showing dewetting patterns. DOPE does not form lamellar structures, so these buds are not GUV buds. Samples were hydrated in PBS doped with 100 mM of sucrose. Scale bar is 10 µm.

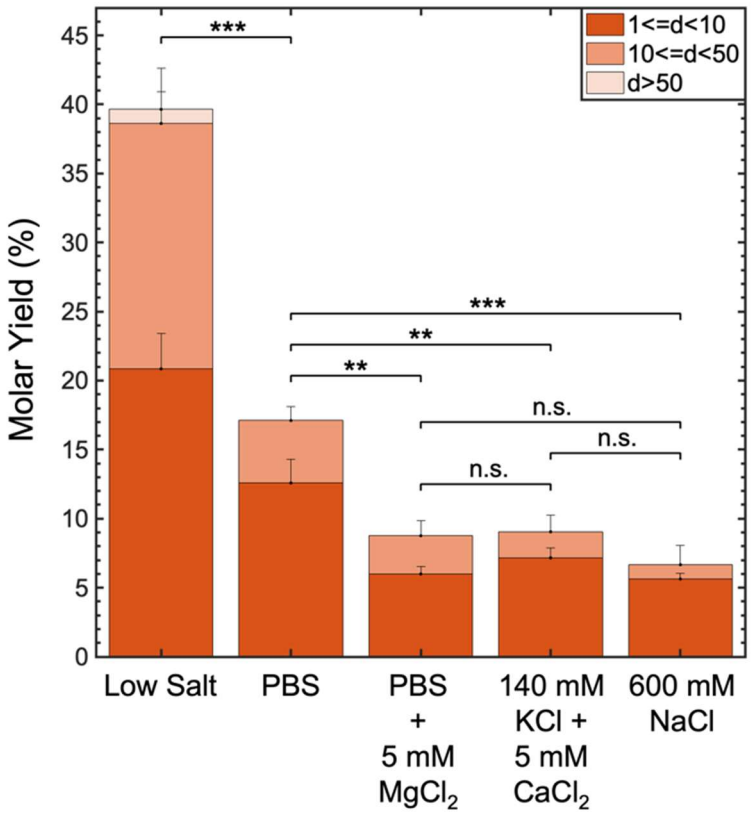

Figure 7. The yield of GUVs depends on the concentration and valency of ions. Stacked bar plot showing yields of GUVs assembled on LGT agarose hydrated in solutions containing low salt, PBS, PBS + 5 mM $MgCl_2$, 140 mM KCl + 5 mM $CaCl_2$, and 600 mM NaCl. The PBS data is reproduced from Figure 2. Each bar is split into 3 regions corresponding to the diameter ranges specified in the legend. Each bar is the average of 3 samples. Statistical significance was determined using a one-way ANOVA and Tukey's HSD posthoc tests. * = $p < 0.05$, ** = $p < 0.01$, *** = $p < 0.001$, ns = not significant. All the buffers containing salts were also doped with 100 mM of sucrose.